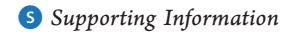


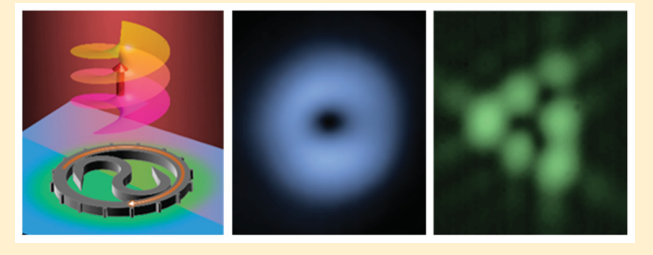
Direct Generation of Tunable Orbital Angular Momentum Beams in Microring Lasers with Broadband Exceptional Points

William E. Hayenga,^{†,‡} Midya Parto,^{†,‡} Jinhan Ren,^{†,‡} Fan O. Wu,[†] Mohammad P. Hokmabadi,[†] Christian Wolff,[§] Ramy El-Ganainy,^{||} N. Asger Mortensen,^{§,±} Demetrios N. Christodoulides,[†] and Mercedeh Khajavikhan*,†,#@

^{*}Ming Hsieh Department of Electrical and Computer Engineering, University of Southern California, Los Angeles 90089, United



ABSTRACT: Non-Hermitian exceptional points (EPs) represent a special type of degeneracy where not only the eigenvalues coalesce, but also the eigenstates tend to collapse on each other. Recent studies have shown that, in the presence of an EP, light-matter interactions are profoundly modified, leading to a host of unexpected optical phenomena ranging from enhanced sensitivity to chiral light transport. Here we introduce a family of unidirectional resonators based on a novel type of broadband exceptional points. In active settings, the resulting unidirectionality exhibits resilience to



perturbations, thus, providing a robust and tunable approach for directly generating beams with distinct orbital angular momenta (OAM). This work could open up new possibilities for manipulating OAM degrees of freedom in applications pertaining to telecommunications and quantum information sciences, while at the same time may expand the notions of non-Hermiticity in the orbital angular momentum space.

KEYWORDS: microresonator, orbital angular momentum, microring laser, non-Hermitian, chirality, exceptional point

I n recent years, there has been a growing interest in the physics and applications of non-Hermitian systems. In wave optics, non-Hermiticity, introduced through gain and loss, leads to novel mechanisms for light generation and transport. The rapid developments in the field of non-Hermitian physics have so far enabled a host of new functionalities, ranging from unidirectional light propagation and robust chiral mode conversion to enhanced sensitivity, to name a few. 2-10 Unique to these systems is a special type of degeneracy, known as an exceptional point, at which not only do the eigenvalues coalesce, but also, their associated eigenvectors become collinear. To a great extent, the recent advances in the field of non-Hermitian photonics can be attributed to our ability to systematically generate such exceptional points in a number of configurations. In this regard, so far, three archetypical arrangements have been identified and widely utilized for generating EPs in microcavities. These include parity-time (PT) symmetric photonic molecules, 8,11,12 PT-symmetric azimuthal gratings, 9 and the incorporation of Rayleigh scatterers in the periphery of a resonator. 7,13-15

The conservation of angular momentum, a direct byproduct of rotational symmetry, plays a pivotal role in physics. In optics, beams carrying orbital angular momentum (OAM) are nowadays finding numerous applications in microscopy, micromanipulation, quantum information, fiber communications, and sensing. 16-34 Over the years, various strategies have been proposed to convert standard beams like Gaussian wavefronts into vortices using off-the-shelf and custom optical components. For example, one can transform an arbitrary wavefront into a vortex OAM beam by manipulating its transverse amplitude/phase profile using appropriately designed phase plates,³⁵ spatial light modulators, computer generated holograms,³⁶ q-plates,³⁷ or metasurfaces.³⁸ In integrated settings, a silicon microring resonator with vertical gratings was found to radiate light with lower-order orbital angular momenta when excited through an adjacent bus waveguide. 39,40 Despite the large body of work on passive

Received: May 29, 2019 Published: August 5, 2019

[†]CREOL, The College of Optics and Photonics, University of Central Florida, Orlando, Florida 32816-2700, United States

[§]Center for Nano Optics, University of Southern Denmark, Campusvej 55, DK-5230 Odense M, Denmark

Department of Physics and Henes Center for Quantum Phenomena, Michigan Technological University, Houghton, Michigan 49931, United States

[⊥]Danish Institute for Advanced Study, University of Southern Denmark, Campusvej 55, DK-5230 Odense M, Denmark

approaches for OAM conversion, the quest for directly generating such twisted beams within a laser cavity has just recently begun. $^{41-43}$

By virtue of their geometry and high index contrast, microring resonators support whispering gallery modes (WGMs) that carry orbital angular momentum. The OAM order (m) is manifested in the azimuthal phase associated with a traveling wave WGM $(e^{im\phi})$. However, due to the rotation symmetry, WGMs are doubly degenerate, that is, an active microring structure simultaneously supports beams with equal positive and negative topological charges, resulting in a net zero OAM generation. Further complications arise when scattering off the cavity walls couples these two counterpropagating modes, resulting in the formation of standing-wave-type bidirectional supermodes. Consequently, in order to be able to use microring lasers for vector vortex generation, it is imperative to break the rotation symmetry between the two counter-propagating modes of the ring.

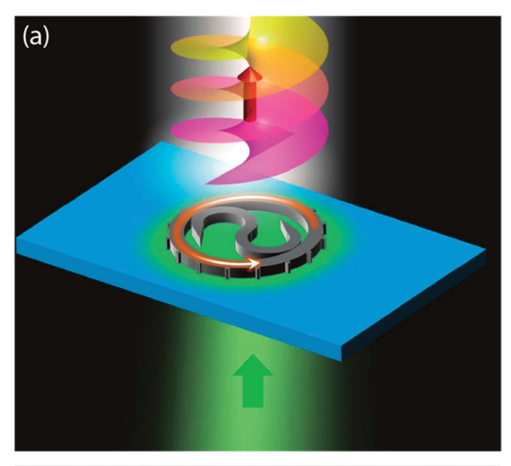
In this work, we introduce the first tunable OAM microring laser based on a new type of non-Hermitian photonic arrangement that supports chiral yet broadband exceptional points. Our proposed structure consists of an active microring resonator with an enclosed S-shaped waveguide with tapered ends. This configuration can be designed in such a way to operate exclusively in the broken phase (above the exceptional point) regime. We further show that the resulting unidirectionality, which is robust against scattering off the walls, can be effectively utilized to demonstrate light sources emitting helical beams with a predetermined topological charge. The robustness of this approach is validated by manipulating the OAM order through grating structures and temperature tuning, thus, for the first time, enabling the realization of a tunable orbital angular momentum laser on a fully integrated III-V semiconductor platform.

■ RESULTS AND DISCUSSION

Establishing Chiral Exceptional Points via Tapered S-Bends in Microring Lasers. To enforce unidirectional operation in active microrings, here we propose to use an S-shaped waveguide with nonreflecting lossy ends inside the resonator. A schematic of this structure with additional corrugations on the exterior cavity walls is depicted in Figure 1a. The two ends of the S-shaped waveguide are adiabatically tapered in order to ensure energy dissipation (radiation loss) and negligible power reflection. As a result, the S-bend provides asymmetric loss/coupling between the two counterpropagating modes. One can readily show that, at resonance, this structure only promotes energy flow in one direction. The asymmetric coupling, caused by the lossy ends of the S-shaped construct, leads to an exceptional point that is inherently chiral, 44,45 with a directionality that can be changed by flipping the cavity upside-down with respect to the substrate.

One can formally justify the formation of such chiral EPs using temporal coupled-mode theory. In a ring with an S-bend similar to that shown in Figure 1a, the modal field amplitudes in the clockwise and counterclockwise directions ($E_{\rm CW}$ and $E_{\rm CCW}$) are related through the following system of coupled differential equations:

$$\begin{cases} \dot{E}_{\rm CW} = i\omega_0 E_{\rm CW} + (g - \gamma) E_{\rm CW} \\ \dot{E}_{\rm CCW} = i\omega_0 E_{\rm CCW} + (g - \gamma) E_{\rm CCW} + i\mu E_{\rm CW} \end{cases} \tag{1}$$



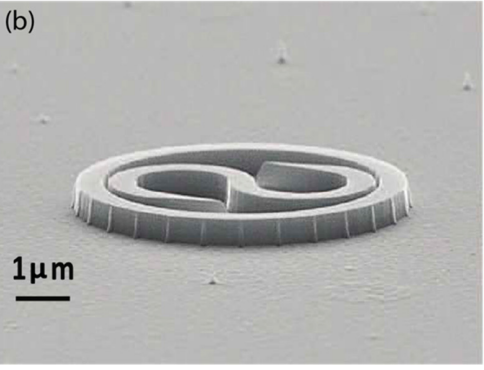
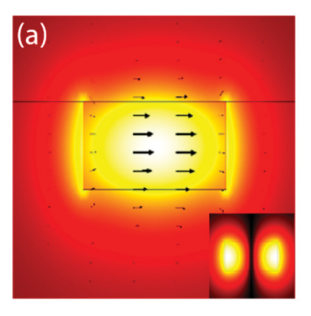


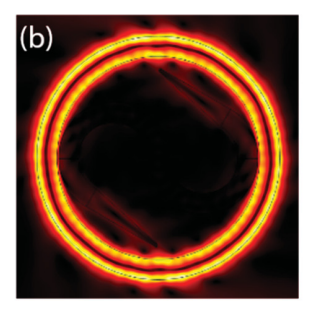
Figure 1. (a) Schematic of the OAM microring laser. (b) SEM image of a fabricated device. The ring has a radius of 3 μ m, a width of 0.5 μ m, and a height of 0.21 μ m. Each scatterer has the dimension of 100 nm \times 100 nm on the top surface.

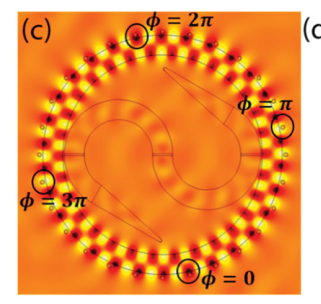
where $E_{\rm CW} = {\rm d}E_{\rm CW}/{\rm d}t$, and so on, ω_0 is the resonant frequency, g is the linear gain, γ represents linear dissipation due to structural/material losses or cavity decay, and μ signifies the unidirectional coupling from the clockwise to the counterclockwise mode. A derivation of eq 1, starting from firstprinciples can be found in Supporting Information, section 1. Even though in this representation, the associated Hamiltonian attains unequal nondiagonal elements, we emphasize that this is by no means an indication of a nonreciprocal behavior. This aspect is discussed further in Supporting Information, section 2. To avoid/reduce scattering losses and other unwanted interference effects, the coupling between the S-bend and the ring is provided through proximity. One can then verify that the Hamiltonian associated with this coupled system is nondiagonalizable, featuring an exceptional point with two identical eigenvalues and eigenvectors, given by

$$\begin{cases} \omega_{1,2} = \omega_0 - i(g - \gamma) \\ |1, 2\rangle = (0,1)^T \end{cases}$$
 (2)

At the EP, this arrangement robustly supports one of the two counter-propagating modes (here the CCW mode), regardless of the lasing wavelength (this aspect is discussed in Supporting Information, section 3). As we will see, this broadband behavior can be advantageously used to facilitate tunable generation of OAM wavefronts. We note that any scattering present in the system (intrinsic or intentional) causes some level of coupling between the two counter-propagating modes,







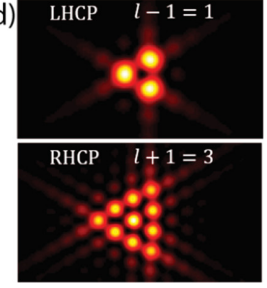


Figure 2. (a) Field intensity of the fundamental TE-mode supported by the cross-sectional waveguide of the microring. The longitudinal mode profile is displayed in the inset. (b) Normalized intensity of the azimuthal component of the E-field inside the structure. (c) Phase evolution of the scatterers located in the outer periphery of the device when l = p - q = 2. (d) Diffraction patterns of left- and right-handed circularly polarized fields through an equilateral triangular aperture.

which in turn forces the system into the broken phase regime, thus, further promoting unidirectionality. Moreover, any additional perturbation that affects both directions in a symmetric fashion has a negligible effect in the resulting unidirectional response. Therefore, as long as generating OAM beams are intended, this idealized model adequately describes the physics. In contrast to previous reports demonstrating unidirectional behavior, where a careful control of the parameters is crucial, the approach proposed here does not require any adjustment. We experimentally validate this robustness by incorporating a grating on the cavity sidewalls to generate low-order OAM beams in a tunable fashion. It should be emphasized that, compared to earlier works, our proposed structure offers several advantages. First, by using the S-bend to impose chirality through an exceptional point in the microring devices, we avoid resorting to other techniques that involve metals. Second, our approach bestows a broadband exceptional point in the structure, which is robust, particularly to the changes in the frequency of operation. Finally, previous studies were, in general, limited to generating a single topological charge, dictated by the geometry of the laser at a specific wavelength. Here, however, our demonstrated OAM microring lasers are capable of generating tunable OAM orders.

Generating OAM Beams with Arbitrary Topological Charges via Sidewall Periodic Scatterers. In order to down-convert the topological charge carried by the WGM of the microcavity and to promote vertical free-space emission, the following angular phase matching condition l = p - q must be satisfied, where $l\hbar$ is the angular momentum per photon associated with this vector vortex beam, p is the WGM number, and q stands for the number of periodic scattering elements along the periphery (the added grating). An OAM microring laser with a radius of 3 μ m, a width of 500 nm, and a height of 210 nm, is fabricated on an InP wafer with InGaAsP quantum wells as the gain material. The width of the S-bend is 500 nm and it is located at a nominal distance of 100 nm at its closest proximity to the ring. Square-shaped protrusions with sides of 100 nm are incorporated along the outermost sidewall of the ring resonator. These scatterers serve as a second-order grating, generating vertical free-space emission with lowerorder twisted beams. Figure 1b displays a scanning electron microscopy (SEM) image of the structure in an intermediate fabrication step. Details pertaining to fabrication can be found in Methods and Supporting Information, section 4.

The modal response of such devices is simulated using finite element methods (FEM). Figure 2a depicts a 2D cross section

of the ring waveguide, supporting the fundamental transverse electric mode (TE₀), which has the highest overlap with the quantum well structure. Correspondingly, the inset of Figure 2a provides the associated longitudinal mode profile. Figure 2b shows a top view of the normalized intensity of the electric field in the ring with a tapered S-bend. The uniform intensity of the electric field (as opposed to a standard standing wave pattern) is an indication of unidirectional power flow in the ring, showing that the exceptional point based device effectively suppresses the backscattering that results in an OAM emission into the order l. In Figure 2b, the chirality of the S-bend was selected so as to promote the CCW mode. The mechanism and function of the tapered S-bend in this work is entirely different from previous reports where Y-junction Sbends are used. Unlike a tapered S-bend that leads to an open configuration, rings with Y-junction S-bends feature conservative systems, where interference effects (as opposed to loss mismtach) are the primary reason for mode suppression.⁴⁶ The OAM conversion process is simulated by including q = 28scattering elements around the periphery of the unidirectional ring (Figure 2c). Considering the resonance condition at 1540 nm (corresponding to p = 30), the vertically extracted field from the scatterers will be given by $\vec{E} \propto \hat{\varphi} e^{il\varphi}$, where l = 2. In order to determine the angular momentum of such a vector vortex beam, the corresponding orthogonal left- and righthanded circularly polarized (L,RHCP) components are identified, each having a topological charge of l-1=1 and l + 1 = 3, respectively, as presented in Figure 2d. Given these two values, one can then deduce the OAM order of the beam to be equal to l = 2.

In order to experimentally measure the topological charge of the microring lasers, a microphotoluminescence (μ -PL) station with additional branches for measuring the OAM order has been employed. The devices are optically pumped by a fiber laser operating at a wavelength of 1064 nm. To accurately measure the OAM beams, the triangular aperture method introduced in ref 47 has been adopted. The far-field diffraction pattern of the emitted beam is assessed upon passing through a circular polarizer (a combination of a quarter-wave plate and a linear polarizer) as well as an equilateral triangular aperture. This triangle-shaped aperture is placed at the back focal plane of a lens, and the InGaAs camera is placed at the front focus. When a beam carrying a nonzero topological charge is incident upon the aperture, a triangular lattice forms that is rotated by $\pm 30^{\circ}$ with respect to the triangle itself. The number of spots along each side is determined by the relationship s = |l| + 1. The direction of the rotation denotes the sign of the OAM

order. More details on the characterization setup can be found in Methods and Supporting Information, section 5. This technique is also compared to the more familiar self-interference approach to establish an equivalence of the two methods. The comparison can be found in Supporting Information, section 6.

In the experiments, we first characterized a microring with a tapered S-bend that supports oscillations in the 27th (p=27) WGM. In order to be able to measure the OAM order, the microring has been equipped with q=26 scattering elements on its sidewall. These scatterers lower the orbital angular momentum of the beam to $l\hbar$ per photon, where l=1. The intensity profile presented in Figure 3a displays the doughnut shape associated with a vortex beam. As expected, the intensity profile of the emission is predominantly azimuthally polarized (Figure 3b). Moreover, using the triangle technique, the OAM characterization indicates a value of l=1, measured by decomposing the beam into two circularly polarized

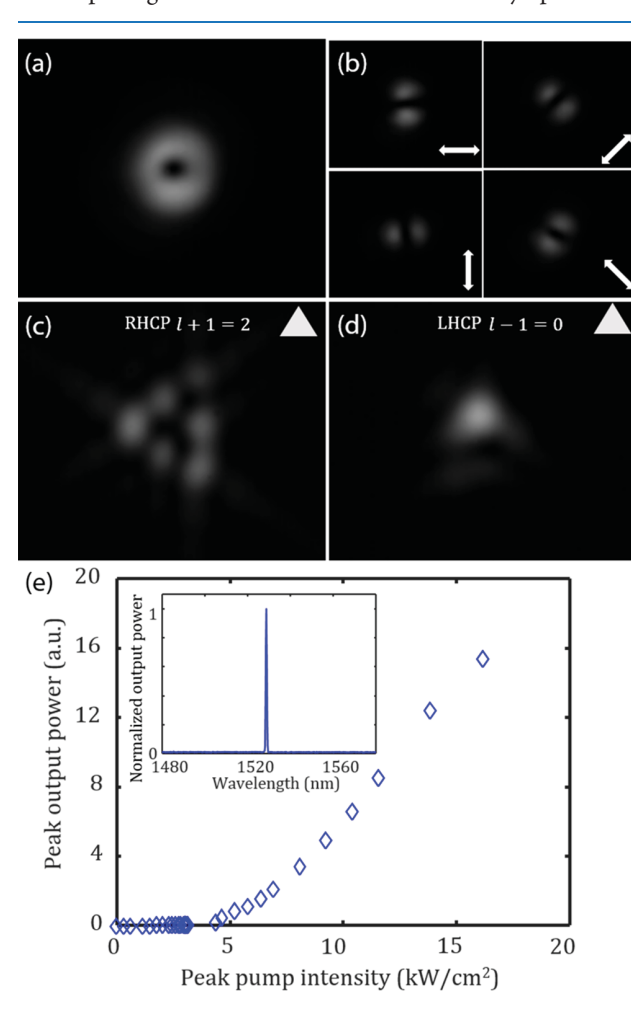


Figure 3. (a) Intensity profile of the microring laser showing a doughnut-shaped beam. (b) Intensity distribution of the lasing emission through a linear polarizer at different orientations (arrows) indicate an azimuthally polarized beam. (c, d) The far-field diffraction pattern of the emission after passing through an equilateral triangle filtered for the right-hand or left-hand circular polarizations, confirming a vortex beam with l = +1. (e) Light-light laser curve, indicating a lasing threshold of 4.1 kW/cm². The inset provides a single-shot spectrum, confirming single-mode lasing at 1529 nm.

components with topological charges of l+1=2 (RHCP) and l-1=0 (LHCP), respectively (Figure 3c,d). Further evidence for unidirectional power flow in rings with tapered Sbends is provided in Supporting Information, section 7. The light–light curve presented in Figure 3e features a threshold behavior characteristic for lasing. A single shot spectrum above threshold is displayed as an inset of Figure 3e, showing a single mode at 1529 nm. Other structures with various radii are fabricated and tested (please see Supporting Information, section 8 for some examples).

To further verify the operating principle of the OAM laser, a number of ring resonators are fabricated with the same radii of 3 μ m (p = 27) but with varying numbers of equally distanced scattering elements (q = 26, 27, and 28) in their peripheries, resulting in the OAM order l = +1, 0, and -1, as depicted in Figure 4a. The measurement results presented in Figure 4b

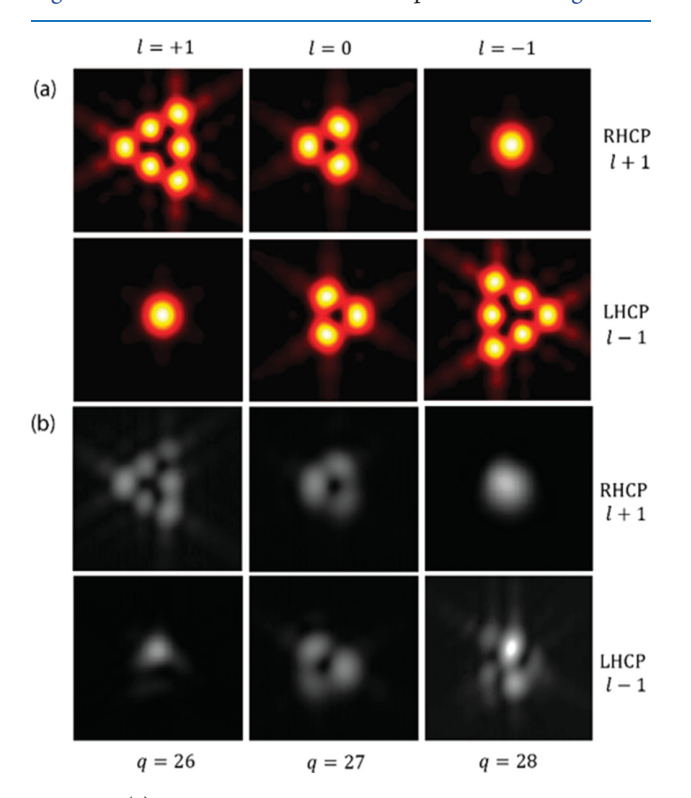


Figure 4. (a) Numerical results for the far-field diffraction of a light beam possessing different OAM orders by an equilateral triangle aperture. (b) The experimental results of the far-field diffraction through the triangle filtered for the RHCP or LHCP, with respect to number of scatterers $q=26,\,27,\,$ and 28. In all cases, the lasers are operating in the p=27 WGM.

clearly confirm the decreased order of topological charge (deviation between simulation and experimental measurements is attributed to a residual ellipticity imparted by the notch filter and beamsplitter). Most notably, when the number of grating pitches is equal to the resonant WGM number of the ring, the resulting emission displays a zero net OAM while remaining an azimuthally polarized vortex beam.

Tuning the Order of the Generated OAM Beam from a Microring Laser. To tune the topological charge of the vector vortex beam, one can use temperature changes. The temperature variations affect the spectral properties of the photoluminescence emission of the gain medium, while at the

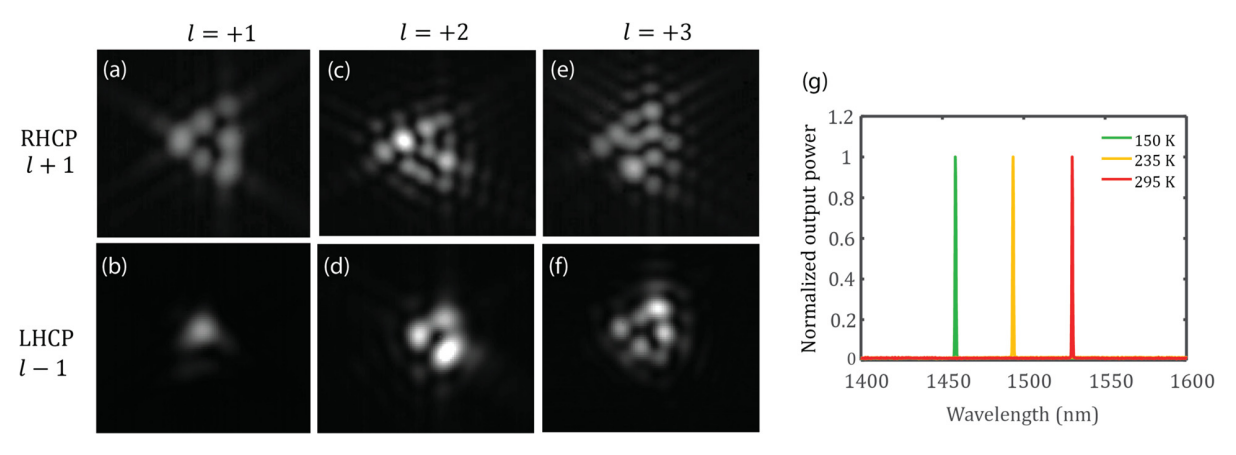


Figure 5. (a, b) Experimental results for the room temperature laser (T = 295 K, p = 27), l = +1 is observed. (c, d) The sample is cooled to T = 235 K, shifting the lasing WGM to the 28th mode. Consequently, the OAM order of the light changes to l = +2. (e, f) The laser is further cooled to T = 150 K (p = 29), resulting in an OAM of l = +3. (g) The corresponding spectrum of the laser at varying temperatures.

same time modifying the resonance condition due to a finite thermo-optic coefficient. Here, the order of the emitted WGM is primarily determined from the resulting shift of the photoluminescence radiation. At a fixed pitch number (q), the change in the number of WGM order (p), directly translates to a change in the topological charge (1). In Figure 5, the temperature tuning of the OAM order has been experimentally demonstrated. At room temperature (295 K), the OAM order of the beam is l = +1 (Figure 5a,b), associated with p = 27 and q = 26. Once its ambient temperature is reduced to 235 K (blue shifting the photoluminescence peak, hence, p = 28), the laser emanates a beam with a different OAM, characterized by l = +2 (Figure 5c,d). Similarly, at a lower temperature of 150 K, the lasing action occurs at 29th WGM, resulting in a topological charge of l = +3 (Figure 5e,f). Figure 5g depicts the emission spectra of lasers generating various OAM orders at different temperatures. The characterization results of a larger ring with a radius of 5 μ m, offering an OAM tuning of 4 orders over 75 K temperature range (295-220 K), is reported in Supporting Information, section 9. The fabrication of yet even larger rings allows for the tuning of the OAM with minimal frequency changes that could potentially be utilized for applications that are not sensitive to limited changes in the wavelength, such as microscopy.

CONCLUSION

In conclusion, in this work we experimentally demonstrated tunable, fully integrated lasers, capable of emitting beams with orbital angular momenta. This was achieved by a realization of exceptional points in microresonators using tapered S-bends. Due to the asymmetric power loss, the S-bend promotes light propagation in one direction, thus leading to a chiral behavior that is robust against perturbations. Our results indicate that this type of microring structures can be used to directly generate vector vortex beams with a predetermined low-order topological charge in a robust fashion. To validate the robustness of this approach, we show that the topological charge can be accurately tuned by adjusting the temperature. Our work features the first realization of on-chip, tunable OAM microring lasers. It may open up new avenues in manipulating and generating OAM beams, with possible applications in sensing, communications, and quantum information sciences, while at the same time harnessing

notions of non-Hermiticity in the orbital angular momentum space.

METHODS

Fabrication. The OAM microring laser is fabricated on III-V semiconductor platform. The gain material consists of six InGaAsP quantum wells with an overall height of 200 nm grown on a p-type InP substrate. The quantum wells are covered by a 10 nm thick InP overlayer for protection. Hydrogen silsesquioxane (HSQ) solution in methyl isobutyl ketone (MIBK) is used as a negative tone electron beam resist. The rings are patterned with electron beam lithography, where the exposed HSQ serves as a mask for the subsequent reactive ion etching process. A mixture of H₂/CH₄/Ar gas chemistry is used with a ratio of 40:10:7 sccm, RIE power of 150 W, and ICP power of 150 W at a chamber pressure of 35 mT. The wafer is then cleaned with oxygen plasma to remove organic contaminations and polymers that form during the dry etching process. The patterns are submerged in buffered oxide etch (BOE) for 10 s to remove the HSQ mask. After this, a 2 μ m layer of SiO2 is deposited onto the wafer using plasmaenhanced chemical vapor deposition (PECVD). SU-8 3010 photoresist is used to bond the wafer to a glass substrate for mechanical support. Lastly, the remaining InP substrate is completely removed by wet etching in hydrochloric acid.

Experimental Arrangement. The OAM microring laser is pumped by a pulsed fiber laser operating at a wavelength of 1064 nm (15 ns pulse width, 290 kHz repetition rate). The pump beam is focused onto the sample with a 50× objective. This objective in turns also collects the emission from the sample. Light is then either directed to a linear array detector for spectral measurements or to an IR camera for modal profile observation. A triangular aperture is inserted at the back focal plane of the lens before the IR camera for OAM measurements.

ASSOCIATED CONTENT

Supporting Information

The Supporting Information is available free of charge on the ACS Publications website at DOI: 10.1021/acsphotonics.9b00779.

Coupled mode analysis of a ring with an S-bend, reciprocity and energy conservation in a passive system,

broadband unidirectionality and robustness analysis, fabrication, characterization setup, comparison of two orbital angular momentum detecting techniques, unidirectional propagation in a microring resonator, measurements of other rings, orbital angular momentum temperature tuning (PDF)

AUTHOR INFORMATION

Corresponding Author

*E-mail: mercedeh@creol.ucf.edu; khajavik@usc.edu.

ORCID [©]

N. Asger Mortensen: 0000-0001-7936-6264 Mercedeh Khajavikhan: 0000-0002-7091-1470

Author Contributions

[‡]These authors contributed equally to this work. W.E.H. and M.K. conceived the idea. J.R. fabricated the samples. M.K., J.R., C.W. and N.A.M. developed the related coupled mode theory, and M.P., J.R., F.W. and W.E.H. designed and analyzed the structures. W.E.H. designed the characterization setup and together with J.R. performed the measurements. All authors contributed in interpreting the results and preparing the manuscript.

Notes

The authors declare no competing financial interest.

ACKNOWLEDGMENTS

National Science Foundation (CBET 1805200, ECCS 1454531, DMR-1420620, ECCS 1757025), Office of Naval Research (N00014-19-1-2052, N0001416-1-2640, N00014-18-1-2347), Air Force Office of Scientific Research (FA9550-14-1-0037), Army Research Office (W911NF-16-1-0013, W911NF-17-1-0481), U.S.—Israel Binational Science Foundation (BSF; 2016381), DARPA (D18AP00058, HR00111820042, HR00111820038), VILLUM Fonden (16498), and H2020 Marie Skłodowska-Curie Actions (MSCA; 713694).

REFERENCES

- (1) El-Ganainy, R.; Makris, K. G.; Khajavikhan, M.; Musslimani, Z. H.; Rotter, S.; Christodoulides, D. N. Non-Hermitian Physics and PT Symmetry. *Nat. Phys.* **2018**, *14*, 11–19.
- (2) Lin, Z.; Ramezani, H.; Eichelkraut, T.; Kottos, T.; Cao, H.; Christodoulides, D. N. Unidirectional Invisibility Induced by PT-Symmetric Periodic Structures. *Phys. Rev. Lett.* **2011**, *106*, 213901.
- (3) Regensburger, A.; Bersch, C.; Miri, M.-A.; Onishchukov, G.; Christodoulides, D. N.; Peschel, U. Parity-Time Synthetic Photonic Lattices. *Nature* **2012**, *488*, 167–171.
- (4) Doppler, J.; Mailybaev, A. A.; Böhm, J.; Kuhl, U.; Girschik, A.; Libisch, F.; Milburn, T. J.; Rabl, P.; Moiseyev, N.; Rotter, S. Dynamically Encircling an Exceptional Point for Asymmetric Mode Switching. *Nature* **2016**, *537*, 76–79.
- (5) Xu, H.; Mason, D.; Jiang, L.; Harris, J. G. E. Topological Energy Transfer in an Optomechanical System with Exceptional Points. *Nature* **2016**, *537*, 80–83.
- (6) Hodaei, H.; Hassan, A. U.; Wittek, S.; Garcia-Gracia, H.; El-Ganainy, R.; Christodoulides, D. N.; Khajavikhan, M. Enhanced Sensitivity at Higher-Order Exceptional Points. *Nature* **2017**, *548*, 187–191.
- (7) Chen, W.; Kaya Özdemir, Ş.; Zhao, G.; Wiersig, J.; Yang, L. Exceptional Points Enhance Sensing in an Optical Microcavity. *Nature* **2017**, *548*, 192–196.
- (8) Hodaei, H.; Miri, M.-A.; Heinrich, M.; Christodoulides, D. N.; Khajavikhan, M. Parity-Time-Symmetric Microring Lasers. *Science* **2014**, 346, 975–978.

(9) Feng, L.; Wong, Z. J.; Ma, R.-M.; Wang, Y.; Zhang, X. Single-Mode Laser by Parity-Time Symmetry Breaking. *Science* **2014**, *346*, 972–975.

- (10) Mortensen, N. A.; Gonçalves, P. a. D.; Khajavikhan, M.; Christodoulides, D. N.; Tserkezis, C.; Wolff, C. Fluctuations and Noise-Limited Sensing near the Exceptional Point of Parity-Time-Symmetric Resonator Systems. *Optica* **2018**, *5*, 1342–1346.
- (11) Peng, B.; Özdemir, Ş. K.; Lei, F.; Monifi, F.; Gianfreda, M.; Long, G. L.; Fan, S.; Nori, F.; Bender, C. M.; Yang, L. Parity-Time-Symmetric Whispering-Gallery Microcavities. *Nat. Phys.* **2014**, *10*, 394–398.
- (12) Brandstetter, M.; Liertzer, M.; Deutsch, C.; Klang, P.; Schöberl, J.; Türeci, H. E.; Strasser, G.; Unterrainer, K.; Rotter, S. Reversing the Pump Dependence of a Laser at an Exceptional Point. *Nat. Commun.* **2014**, *5*, 4034.
- (13) Wiersig, J. Structure of Whispering-Gallery Modes in Optical Microdisks Perturbed by Nanoparticles. *Phys. Rev. A: At., Mol., Opt. Phys.* **2011**, 84, 063828.
- (14) Wiersig, J.; Kim, S. W.; Hentschel, M. Asymmetric Scattering and Nonorthogonal Mode Patterns in Optical Microspirals. *Phys. Rev. A: At., Mol., Opt. Phys.* **2008**, *78*, 053809.
- (15) Wiersig, J. Sensors Operating at Exceptional Points: General Theory. *Phys. Rev. A: At., Mol., Opt. Phys.* **2016**, 93, 033809.
- (16) Padgett, M. J. Orbital Angular Momentum 25 Years on. *Opt. Express* **2017**, 25, 11265–11274.
- (17) Fürhapter, S.; Jesacher, A.; Bernet, S.; Ritsch-Marte, M. Spiral Interferometry. *Opt. Lett.* **2005**, *30*, 1953–1955.
- (18) Gahagan, K. T.; Swartzlander, G. A. Optical Vortex Trapping of Particles. Opt. Lett. 1996, 21, 827–829.
- (19) Grier, D. G. A. Revolution in Optical Manipulation. *Nature* 2003, 424, 810.
- (20) Mair, A.; Vaziri, A.; Weihs, G.; Zeilinger, A. Entanglement of the Orbital Angular Momentum States of Photons. *Nature* **2001**, *412*, 313
- (21) Bozinovic, N.; Yue, Y.; Ren, Y.; Tur, M.; Kristensen, P.; Huang, H.; Willner, A. E.; Ramachandran, S. Terabit-Scale Orbital Angular Momentum Mode Division Multiplexing in Fibers. *Science* **2013**, *340*, 1545–1548.
- (22) Kravets, V. G.; Schedin, F.; Jalil, R.; Britnell, L.; Gorbachev, R. V.; Ansell, D.; Thackray, B.; Novoselov, K. S.; Geim, A. K.; Kabashin, A. V.; et al. Singular Phase Nano-Optics in Plasmonic Metamaterials for Label-Free Single-Molecule Detection. *Nat. Mater.* **2013**, *12*, 304–309
- (23) Zhang, W.; Wei, K.; Huang, L.; Mao, D.; Jiang, B.; Gao, F.; Zhang, G.; Mei, T.; Zhao, J. Optical Vortex Generation with Wavelength Tunability Based on an Acoustically-Induced Fiber Grating. *Opt. Express* **2016**, *24*, 19278–19285.
- (24) Lyubopytov, V. S.; Porfirev, A. P.; Gurbatov, S. O.; Paul, S.; Schumann, M. F.; Cesar, J.; Malekizandi, M.; Haidar, M. T.; Wegener, M.; Chipouline, A.; et al. Simultaneous Wavelength and Orbital Angular Momentum Demultiplexing Using Tunable MEMS-Based Fabry-Perot Filter. *Opt. Express* 2017, 25, 9634–9646.
- (25) Liu, Q.; Zhao, Y.; Ding, M.; Yao, W.; Fan, X.; Shen, D. Wavelength- and OAM-Tunable Vortex Laser with a Reflective Volume Bragg Grating. *Opt. Express* **2017**, *25*, 23312–23319.
- (26) Yao, S.; Ren, G.; Shen, Y.; Jiang, Y.; Zhu, B.; Jian, S. Tunable Orbital Angular Momentum Generation Using All-Fiber Fused Coupler. *IEEE Photonics Technol. Lett.* **2018**, *30*, 99–102.
- (27) Shen, Y.; Meng, Y.; Fu, X.; Gong, M. Wavelength-Tunable Hermite-Gaussian Modes and an Orbital-Angular-Momentum-Tunable Vortex Beam in a Dual-off-Axis Pumped Yb:CALGO Laser. *Opt. Lett.* **2018**, *43*, 291–294.
- (28) Shen, Y.; Meng, Y.; Fu, X.; Gong, M. Dual-Wavelength Vortex Beam with High Stability in a Diode-Pumped Yb:CaGdAlO4 Laser. *Laser Phys. Lett.* **2018**, *15*, 055803.
- (29) Wang, S.; Zhang, S.; Li, P.; Hao, M.; Yang, H.; Xie, J.; Feng, G.; Zhou, S. Generation of Wavelength- and OAM-Tunable Vortex Beam at Low Threshold. *Opt. Express* **2018**, *26*, 18164–18170.

(30) Zhou, N.; Liu, J.; Wang, J. Reconfigurable and Tunable Twisted Light Laser. Sci. Rep. 2018, 8, 11394.

- (31) Mock, A.; Sounas, D.; Alù, A. Tunable Orbital Angular Momentum Radiation from Angular-Momentum-Biased Microcavities. *Phys. Rev. Lett.* **2018**, *121*, 103901.
- (32) Zhou, N.; Zheng, S.; Cao, X.; Gao, S.; Li, S.; He, M.; Cai, X.; Wang, J. Generating and Synthesizing Ultrabroadband Twisted Light Using a Compact Silicon Chip. *Opt. Lett.* **2018**, *43*, 3140–3143.
- (33) Xie, Z.; Lei, T.; Li, F.; Qiu, H.; Zhang, Z.; Wang, H.; Min, C.; Du, L.; Li, Z.; Yuan, X. Ultra-Broadband on-Chip Twisted Light Emitter for Optical Communications. *Light: Sci. Appl.* **2018**, *7*, 18001.
- (34) Rodríguez-Fortuño, F. J.; Barber-Sanz, I.; Puerto, D.; Griol, A.; Martínez, A. Resolving Light Handedness with an On-Chip Silicon Microdisk. *ACS Photonics* **2014**, *1*, 762–767.
- (35) Beijersbergen, M. W.; Coerwinkel, R. P. C.; Kristensen, M.; Woerdman, J. P. Helical-Wavefront Laser Beams Produced with a Spiral Phaseplate. *Opt. Commun.* **1994**, *112*, 321–327.
- (36) Heckenberg, N. R.; McDuff, R.; Smith, C. P.; White, A. G. Generation of Optical Phase Singularities by Computer-Generated Holograms. *Opt. Lett.* **1992**, *17*, 221–223.
- (37) Karimi, E.; Piccirillo, B.; Nagali, E.; Marrucci, L.; Santamato, E. Efficient Generation and Sorting of Orbital Angular Momentum Eigenmodes of Light by Thermally Tuned Q-Plates. *Appl. Phys. Lett.* **2009**, *94*, 231124.
- (38) Yu, N.; Genevet, P.; Kats, M. A.; Aieta, F.; Tetienne, J.-P.; Capasso, F.; Gaburro, Z. Light Propagation with Phase Discontinuities: Generalized Laws of Reflection and Refraction. *Science* **2011**, 334, 333–337.
- (39) Cai, X.; Wang, J.; Strain, M. J.; Johnson-Morris, B.; Zhu, J.; Sorel, M.; O'Brien, J. L.; Thompson, M. G.; Yu, S. Integrated Compact Optical Vortex Beam Emitters. *Science* **2012**, 338, 363–366.
- (40) Strain, M. J.; Cai, X.; Wang, J.; Zhu, J.; Phillips, D. B.; Chen, L.; Lopez-Garcia, M.; O'Brien, J. L.; Thompson, M. G.; Sorel, M.; et al. Fast Electrical Switching of Orbital Angular Momentum Modes Using Ultra-Compact Integrated Vortex Emitters. *Nat. Commun.* **2014**, *S*, 4856.
- (41) Naidoo, D.; Roux, F. S.; Dudley, A.; Litvin, I.; Piccirillo, B.; Marrucci, L.; Forbes, A. Controlled Generation of Higher-Order Poincaré Sphere Beams from a Laser. *Nat. Photonics* **2016**, *10*, 327–322
- (42) Miao, P.; Zhang, Z.; Sun, J.; Walasik, W.; Longhi, S.; Litchinitser, N. M.; Feng, L. Orbital Angular Momentum Microlaser. *Science* **2016**, 353, 464–467.
- (43) Peng, B.; Özdemir, Ş. K.; Liertzer, M.; Chen, W.; Kramer, J.; Yılmaz, H.; Wiersig, J.; Rotter, S.; Yang, L. Chiral Modes and Directional Lasing at Exceptional Points. *Proc. Natl. Acad. Sci. U. S. A.* **2016**, *113*, 6845–6850.
- (44) Ren, J.; Liu, Y. G. N.; Parto, M.; Hayenga, W. E.; Hokmabadi, M. P.; Christodoulides, D. N.; Khajavikhan, M. Unidirectional Light Emission in PT-Symmetric Microring Lasers. *Opt. Express* **2018**, *26*, 27153–27160.
- (45) Bandres, M. A.; Wittek, S.; Harari, G.; Parto, M.; Ren, J.; Segev, M.; Christodoulides, D. N.; Khajavikhan, M. Topological Insulator Laser: Experiments. *Science* **2018**, *359*, No. eaar4005.
- (46) Hohimer, J. P.; Vawter, G. A.; Craft, D. C. Unidirectional Operation in a Semiconductor Ring Diode Laser. *Appl. Phys. Lett.* **1993**, *62*, 1185–1187.
- (47) Hickmann, J. M.; Fonseca, E. J. S.; Soares, W. C.; Chávez-Cerda, S. Unveiling a Truncated Optical Lattice Associated with a Triangular Aperture Using Light's Orbital Angular Momentum. *Phys. Rev. Lett.* **2010**, *105*, 053904.